Stony Brook University

Nanoscale eengineering of infrared plasmons in graphene

A Thesis presented

by

Haiming Deng

to

The Graduate School

in Partial Fulfillment of the

Requirements

for the Degree of

Master of Arts

in

Physics

Stony Brook University

May 2016

Stony Brook University

The Graduate School

Haiming Deng

We, the thesis committe for the above candidate for the

Master of Arts degree, hereby recommend

acceptance of this thesis

Prof. Xu Du - Thesis Advisor
Associate Professor, the Department of Physics and Astronomy

Prof. Mengkun Liu - Second Reader
Assistant Professor, the Department of Physics and Astronomy

Prof. Dmitri Kharzeev - Third Reader
Professor, the Department of Physics and Astronomy

This thesis is accepted by the Graduate School

Charles Taber
Dean of the Graduate School

Abstract of the Thesis

Plasmon Study of Graphene

by

Haiming Deng

Master of Arts

in

Physics

Stony Brook University

2016

Surface plasmons are collective oscillations of free charge carriers confined in interface between two dielectrics, where the real part of the dielectric changes sign (e.g a metal-insulator interface such as gold film and air). The study of surface plasmon has been a popular research theme with potential applications utilizing the fact that the wavelength of plasmons can be many order smaller than that of the incident lights. The potential applications include transfer of information in hundreds of terahertz instead of upper limit of gigahertz in traditional wires, photodetectors with frequency range from terahertz to mid-IR, and nano-imaging. In our experiment, we use an IR near-field microscopy with resolution as low as 10nm but energy scale of micron range. This is achieved by shinning an AFM tip with infrared laser on top of the sample and collecting the scattered light from the sample. The spatial resolution proportional to where a is the size of the tip and the resolution can reach 10nm. This technique beats the diffraction limit of near-IR (10um) by over 1000x. The wavelength and amplitude damping of plasmon greatly depends on the property of free carriers in the material. While metals such as gold had been widely studied and shown promising results, a better platform with longer propagation length and shorter wavelength is needed for application. Graphenes supreme electronic transport property makes it ap-

pears to be an excellent candidate for plasmonic. Graphene plasmon across a p-n junction will be discussed. Oxygen doping of graphene with different dosage via UV ozone is studied. Oxygen doping has shown promising results for graphene plasmon guide. Plasmon fringes are developed in the interior breaking the limit of boundary condition. The UV ozone treatment can be fine controlled and without damaging the graphene sheet. One can, in theory, mask and selectively dope to create a robust graphene plasmon circuit that is stable in room temperature.

Table of Contents

List of Figures

Chapter 1   Introduction

Plasmons are collective oscillations of free charge carriers confined in interface between two dielectrics, where the real part of the dielectric changes sign, for example a metal-insulator interface such as gold and air. A plasmon can be viewed as a quasiparticle since it arises from the quantization of plasma oscillations, just like that phonons are quantizations of lattice vibrations. Surface plasmon polariton (SPP) is another quasiparticle resulted from the coupled state of plasmon inside the conducting sheet and surface electromagnetic wave generated by plasmon on the 2D interface of metal insulator. Thought out this paper, for clarification, we will use a slightly modified meaning of the word "meta" which in band theory is classified as materials which have partially filled electronic states of overlapped conducting and valence band. In here however, metal means materials with free carriers, which can be metals, semimetals or semiconductors with fermi level deep into the conducting band.

One of the most interesting things about SPP is the mechanism of propagation. SPP travels on the surface of the metal while its associated plasmon is inside the metal. Intuitively, a harmonic electromagnetic (EM) wave is generated by the free carriers collective oscillations inside the metal whose wavelength is limited by electronic properties of the carrier such as its mobility, carrier concentration and the photon absorption spectrum from the phonons. As a result, the energy dispersion curve of SPP is nonlinear and its curvature depends not just on the dielectric constant of the metal but also electronic properties of the metal. Moreover, curvature of the dispersion allows various plasmon wavelength differ from the incident light. Theoretically, the wavelength of plasmon on the metal can be over thousand times shorter than the incident light, making it potentially valuable in sub-wavelength imaging. Ordinarily, the spatial resolution of an optical device is limited by its diffraction limit, that is, the wavelength of light, which is at best on the order of a micrometer. And this scale is often too large to observe localized effects such as defects and local dopants, which often play important roles in the collective electronic property of the material. Another reason plasmon has attracted so much attention in recent years is that it allow the study of same material with unaltered spatial resolution but in different energy scale. This has expanded plasmonic field dramaticly becasue ,without worrying about the diffraction limit, one now has the freedom to to excite free charge carriers using photon with different energy into the exact energy levels

and study the dynamic of the charge carrier in non-equilibrium state. One particular favored range is infrared regime because of its low energy scale matches many of the novel materials that shows exotic behaviors.(i.e topological insulators and graphene). This has opened up the ability to study small excitations of charge carriers out of equilibrium. This sub-wavelength is fundamentally important in study of novel materials with small band gap, local effects and nano-scale application.

In our experiment, we utilized the sub-wavelength property of SPPs to study plasmon on graphene sandwiched by hexagonal boron nitride (hBN), detecting defects and oxygen dopants of graphene in nano-scale with plasmon. And we also explored the possibility of confining SPPs on graphene by using a potential well, created with a sharp p-n junction by gating.distances.

Chapter 2   Fundamentals

In this chapter, we will be going over some basic concepts of Surface plasmon polariton (SPP).

2.1   Derivation of SPP and BPP dispersion curve

As we already mentioned in the introduction, SPPs are electromagnetic (EM) waves trapped at the surface of a metal. Let $z = 0$ defines a surface between a metal with dielectric function $\varepsilon_m(\omega)$ and a dielectric with dielectric constant $\varepsilon_d(\omega)$. Under certain conditions, this system can support EM wave of frequency ω propagating along the surface of metal. The schematic set up is shown in Fig. 1. If we write for the EM fields $E_d(z > 0) \propto e^{i(k_{xd}x + k_{zd}z - wt)}$ above the metal, and $E_d(z < 0) \propto e^{i(k_{xm}x + k_{zm}z - wt)}$. The boundary condition at $z = 0$ requires the EM field to be continues, this gives the corresponding relation between k_m and k_d

$$\frac{k_{zd}}{\varepsilon_d} + \frac{k_{zm}}{\varepsilon_m} = 0 \tag{1}$$

In general, light traveling in a dielectric ε has the wavelength and frequency relation $k^2 = \varepsilon \frac{\omega^2}{c^2}$, and $k^2 = k_z^2 + k_x^2$. Also, at the interface, $k_{xd} = k_{xm} \equiv k_x$. So we can write

$$k_x^2 + k_{zd}^2 = \varepsilon_d \frac{\omega^2}{c^2}, \tag{2}$$

$$k_x^2 + k_{zm}^2 = \varepsilon_m \frac{\omega^2}{c^2}. \tag{3}$$

From relations above, one can obtain the following dispersion relations of k_x, k_{zd} and k_{zm}:

$$k_x^2 = \left(\frac{\omega}{c}\right)^2 \frac{\varepsilon_m \varepsilon_d}{\varepsilon_m + \varepsilon_d}, \tag{4}$$

$$k_{zd}^2 = \left(\frac{\omega}{c}\right)^2 \frac{\varepsilon_d^2}{\varepsilon_m + \varepsilon_d}, \tag{5}$$

$$k_{zm}^2 = \left(\frac{\omega}{c}\right)^2 \frac{\varepsilon_m^2}{\varepsilon_m + \varepsilon_d}. \tag{6}$$

As is shown in Fig. 1, the EM wave decays exponentially in the z-direction. So the SPP dispersion relation is dominated by equation (4) in
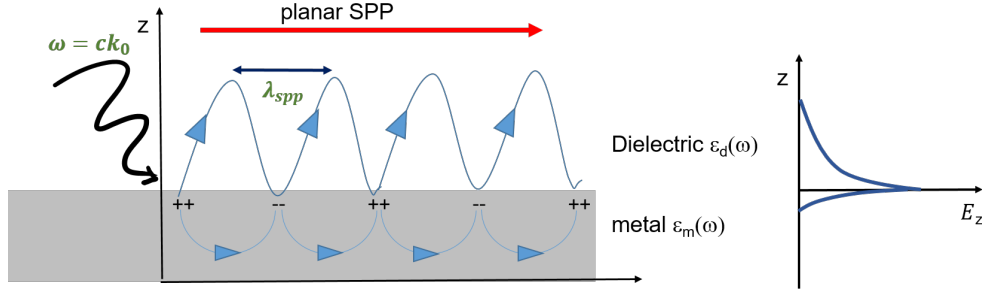
Figure 1: Schematic drawing of a SPP at a metal-insulator interface. The collective oscillations of free charge carriers inside metal generate an EM wave on the surface decaying exponentially in the z-direction. The SPP is confined on the surface of the metal.

the direction along the metal surface, which gives for SSP

$$\omega = \sqrt{\frac{\varepsilon_m + \varepsilon_d}{\varepsilon_m \varepsilon_d}} c k_x. \tag{7}$$

As you might see from the dispersion curve, compared with the dispersion of photon in air, such a dispersion curve is similar but with a factor of ratio of dielectrics difference in front. Another thing to note is, inside the metal, the dielectric constant is a function of frequency ω, which is exactly where the curvature comes from.

In the following part, we will show briefly how to derivate, from the Drude model, the dispersion of Plasmon inside the bulk of the metal. In the Drude approximation, a metal has electron liquid of high density $n \approx 1023 \mathrm{cm}^{-3}$. And a longitudinal density oscillation, i.e. a plasmon, with frequency ω_p will have quantized energy

$$\hbar \omega_p = \hbar \sqrt{\frac{n e^2}{m_0 \varepsilon_0}}. \tag{8}$$

An EM wave can propagate through the bulk of metal for frequency $\omega > \omega_p$. So there will be bulk plasmon polaritons (BPPs) with certain dispersion relations. The dielectric function in Drude metal has the following frequency relation

$$\varepsilon_m = 1 - \frac{\omega_p^2}{\omega^2}. \tag{9}$$

4
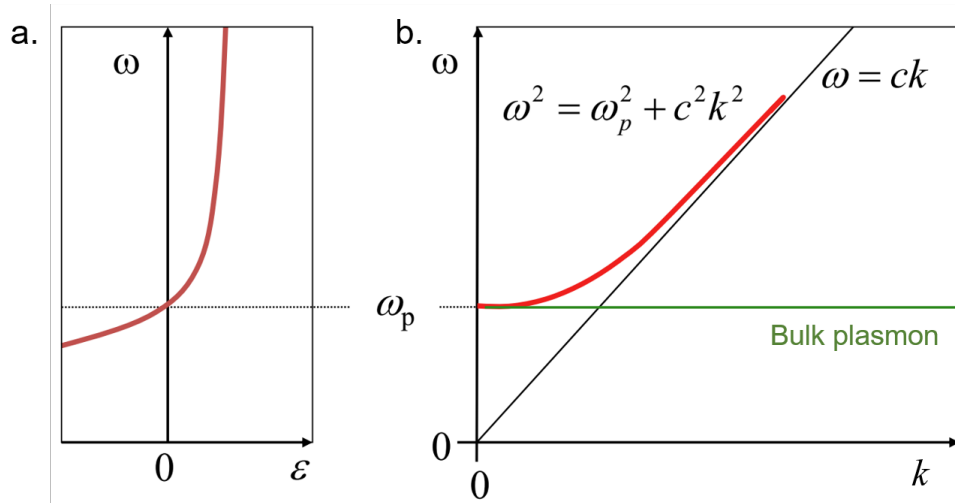
Figure 2: a. Schematic drawing of ω, for a Drude metal, as a function of ε. As shown in the graph, $\varepsilon = 0$ for $\omega = \omega_p$ (the plasmon frequency). And when $\omega < \omega_p$, the dielectric ε of the metal is negative, which is an important reason why the dispersion curve for SPP is curved away from the photon dispersion curve and hosts many interesting and unexplored phenomena of SPP; b. plot of BPP dispersion from Drude approximation of plasmon traveling in a high density electron liquid. When $\omega \ll \omega_p$, the dispersion curve approaches the photon line.

Along with $k^2 = \varepsilon \frac{\omega^2}{c^2}$, the bulk plasmon polariton can be rewritten as

$$\omega^2 = \omega_p^2 + c^2 k^2. \tag{10}$$

Fig. 2 shows the ω's dependence on ε for a Drude metal, which is valid for both BPPs and SPPs, and the dispersion curve of BPPs.

Now putting together both results for surface and bulk plasmon polariton, the resulted dispersion curve is shown in Fig. 3. As ω gradually approaches $\omega_p/\sqrt{1 + \varepsilon_d}$, called the surface plasmon resonant frequency, a plasmon in the metal and a photon couple together on the surface of the metal and become a SPP asymptotically. This occurs when relative permittivities of the metal and the dielectric are of the same magnitude but opposite sign, which produces a pole in the dispersion relation, as is shown in equation (4). Generally, for highly conductive thin film like gold and silver, dispersion relation lines
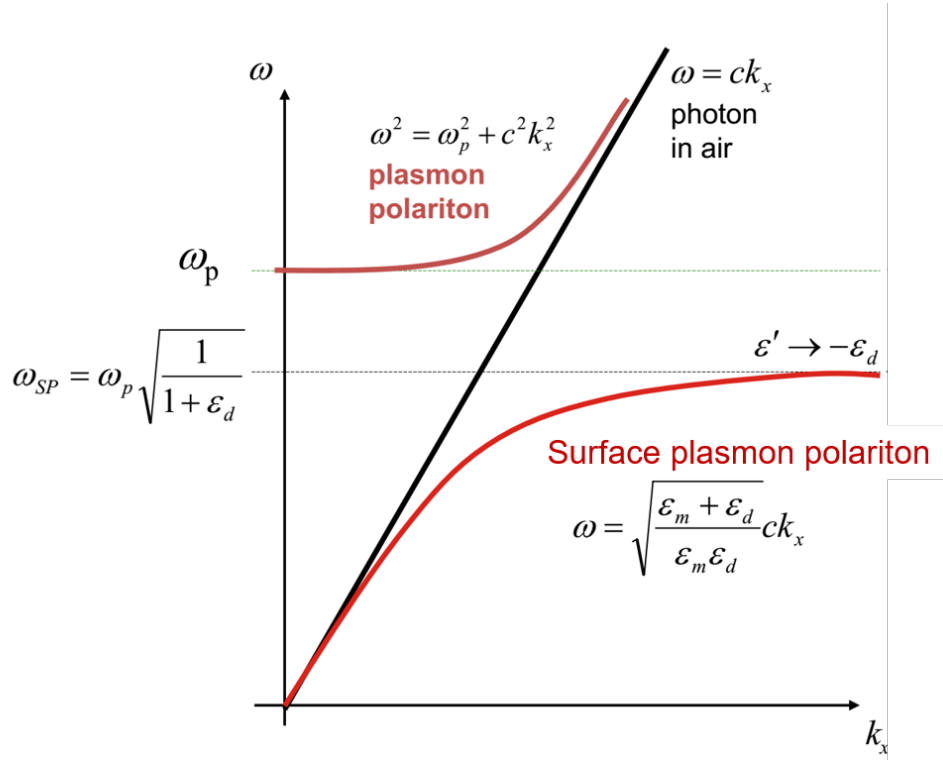
Figure 3: Schematic dawing to show a the behavior of a dispersion curve for surface plasmon polaritons (SPPs,red) and bulk plasmon polaritons (BPPs, red) respect to the photon line (black). At low k, the SPP curve approaches the photon line and the BPP curve approaches the bulk plasmon frequency ω_p. At high k, the SPP curve approaches $\varepsilon'\omega_p$, where ε' is a factor less than 1 and depends on the dielectric constant above the metal. In this convention, the dielectric is always real and positive while the dielectric of the metal is negative. This is true as has been shown above in the Drude model.

of SPP and photon are very close until visible and near-IR regime, implying that the wavelength associated with the SPP in these regimes is only slightly shorter than that of light of the same frequency. However, knowledge we knew in this field is still limited and in some exotic material, e.g. graphene, SPP can have a wavelength of the order of 100nm in near-IR ($\sim 10\mu$m) regime, and the ratio λ/λ_0 is as much as 1000. In theory the ratio λ/λ_0 can reach the order of thousand and even higher in unexplored materials.

2.2 Propagation length and skin depth

As we have briefly mentioned earlier, SPP decays exponentially in the direction away from the metal and dissipates its energy to scatterings and phonon vibrations as it propagates. We will derive these result quantitatively here.

A SPP wave is a plane wave in perfectly flat metal surface and travels in one direction (i.e. away from the boundary). In Maxwells EM theory, any propagating EM plane waves in the x-direction can be written as

$$E = E_0 e^{ik_x x}. \tag{11}$$

where k_x is real. If k_x is complex, there will be an exponentially decay term coming from the imaginary part of k_x. We didnt mention in above sessions but our momentum is complex in general, as both real and imaginary part matter here. In order to separate the propagating real k_x from the exponentially damping term, we write $k_x = k'_x + ik''_x$.

Starting from the complete equation of relative permittivity given in Drude model of a simple metal (with imaginary part)

$$\varepsilon_m = 1 - \frac{\omega_p^2}{\omega^2 - i\gamma\omega}, \tag{12}$$

where γ is the scattering rate that is used to account for dissipation through scattering of the electron motion, the dielectric of the metal has both real and imaginary part. Define $\varepsilon_m = \varepsilon'_m + i\varepsilon''_m$, one can plot its real and imaginary part as function of ω/ω_p as is shown in Fig. 4.

Now according to the dispersion relation for SPPs, say equation (7),

$$k_x = k'_x + ik''_x = \frac{\omega}{c}\sqrt{\frac{\varepsilon_m \varepsilon_d}{\varepsilon_m + \varepsilon_d}}. \tag{13}$$

Plug k_x back into equation (11)

$$E = E_0 e^{-k''_x x} e^{ik'_x x}, \tag{14}$$

7
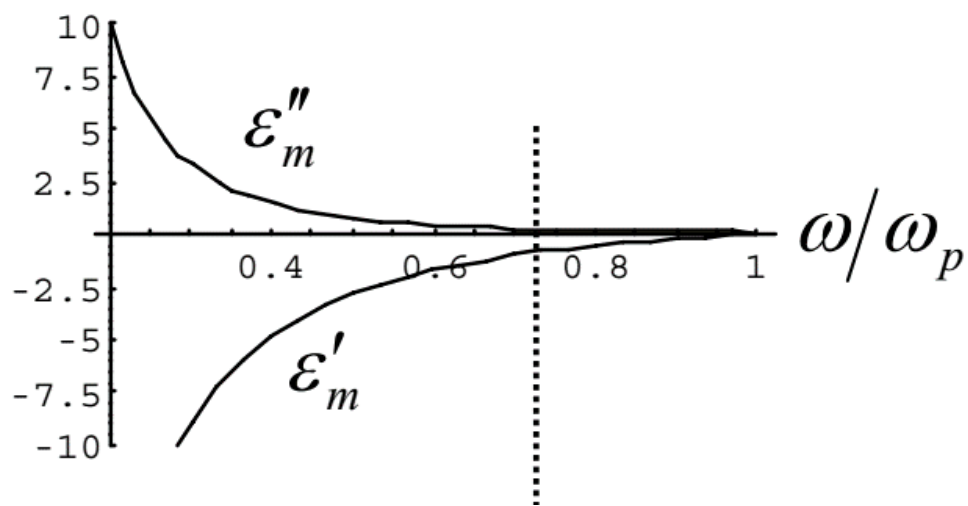
Figure 4: Real and imaginary part of the dielectric of metal as function of ω/ω_p. The real part is always negative and larger than the imaginary part. It agrees with negative dielectric of metal required for SPP. The dash line is where the imaginary part dies off as ω is approaching $\omega_{sp} = \omega_p/\sqrt{2}$, as the graph is plotted with $\gamma = 0.2$. Note thatthe graph is obtained from online lecture note of applied optics by A. La Rosa at Portland State University

where the first term is the propagation term of the SPP and second term is the exponential decay term in the direction of the propagation. The propagation length is just inverse of the decay rate. Because we are looking at the intensity not the amplitude of the EM wave, a factor of 2 should be added. All together, the propagation length is then

$$L_x = \frac{1}{2k_x''}.$$ (15)

According to equation (13), one can see k_x is a function of the damping term γ. This shows that the scattering strength is crucial to the propagation length. Defects, the electron-electron interaction and electron-phonon interactions indirectly play crucial roles of the propagation length of plasmon. It is more illustrative to show only the imaginary part of the wave number k_x'' in terms of dielectrics:

$$k_x'' = k_0 \frac{\varepsilon_m''}{\varepsilon_m'^2} \sqrt{\frac{\varepsilon_m' \varepsilon_d}{\varepsilon_m' + \varepsilon_d}}^3,$$ (16)

given photon in the dielectric medium $k_0 = \omega c$, which gives the propagation length

$$L_x = \lambda_0 \frac{\varepsilon_m'^2}{2\pi \varepsilon_m''} \left(\frac{\varepsilon_m' \varepsilon_d}{\varepsilon_m' + \varepsilon_d} \right)^{-\frac{3}{2}}.$$ (17)

A few remarks can be made by interpreting equation (17). For simplicity, for a highly conductive metal thin film, the real part of the dielectric of the metal ε_m' is large and if we take the dielectric to be vacuum/air one can approximate $\varepsilon_m' \ll \varepsilon_d$, which gives $L_x = \lambda_0 \frac{\varepsilon_m'^2}{2\pi \varepsilon_m''}$. As we can see from Figure 4, the ratio $\varepsilon_m'^2 / \varepsilon_m''$ will be large for $\sqrt{2}\omega < \omega_p$. This implies that the propagation length will be much longer than the wavelength of light in free space and in term implies $L_x \ll \lambda_{\text{SPP}}$. To show this as an example, we will refer to the L_x over λ_{SPP} plot for silver calculated with Drude model in Barnes review paper in Fig. 5. [?]

Barnes' plot of propagation length in Fig. 5 used a simplified version of equation (17) and was based on Drude parameters for silver in visible and near-IR regime. The propagation length in the plot is many order larger than the SPP wavelength.

9
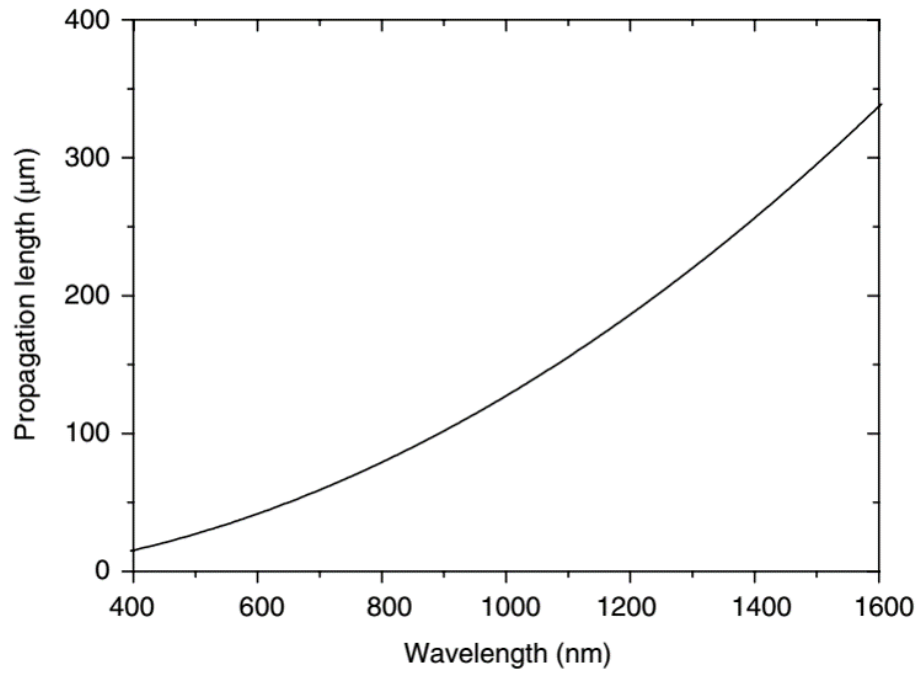
Figure 5: Propagation length of SPP. The data were computed using Drude approximation for the relative permittivity of silver ($\omega_p = 1.2 \times 10^{16}$rad/s and $\gamma = 1.45 \times 10^{13}$). The relative permittivity of the dielectric was taken to be 1. (This plot is from Barnes 2006[12])

Now we continue to the skin depth of SPP. As we have mentioned briefly above as well as seen from Fig. 1, penetrations into both the dielectric and metal decay exponentially with different damping factors depending on the dielectric values. In general

$$E_z = E_0 e^{-k_z'' x}, \tag{18}$$

and

$$L_z = \frac{1}{k_z''}. \tag{19}$$

where k_z'' is, similar to the x-direction case, the imaginary part of the z-component wave-vector. The relation between k_z, k_{SPP} and k_0 is as following:

$$\varepsilon_i k_0^2 = k_{\text{SPP}}^2 + k_{z,i}^2, \tag{20}$$

where $i = d, m$ representing the corresponding dielectric. As we noted above, the wavelength of a SPP is always shorter than that of a photon traveling in the adjacent medium. This implies $k_{\text{SPP}}^2 > \varepsilon_i k_0^2$. So that the z-component of the wave-vector in both media is imaginary, representing the exponentially fall off of the fields with distance into the media. For clarification, the longitudinal wave-vector k_x is the wave vector of SPP as is shown in the set up in Fig. 1. But from now we will use k_{SPP} as a more symbolic representation. Now combining the dispersion relation of k_{SPP} from equation (2), the penetration depth in the two media are then:

$$L_d = \frac{1}{k_0} \left| \frac{\varepsilon_m' + \varepsilon_d}{\varepsilon_d^2} \right|^{1/2}, \tag{21}$$

$$L_m = \frac{1}{k_0} \left| \frac{\varepsilon_m' + \varepsilon_d}{\varepsilon_m'^2} \right|^{1/2}. \tag{22}$$

For reference, when calculating using Drude model of silver with $\gamma = 0.2$ and $\varepsilon_d = 1$, and with wavelength $\lambda_0 = 600$nm, $L_{z,d} = 390$nm and $L_{z,m} = 24$nm, the skin depth of the metal is much smaller than that in the dielectric. One outlook is to note that the penetration depth in dielectric is relatively long compared to the SPP wavelength. One can place two metal sheets closely together with a separation less than the penetration depth and couple the SPP between the two sheets to create a resonant condition which can enhance

11

the amplitude and extend the range of propagation. In theory, the problem of finite propagation length can be overcomed by engineering array of identical metal sheets, which, however, still faces many difficulties to engineer such systems.

Chapter 3   Apparatus and Experiments

3.1   Apparatus

Our main apparatus used to launch plasmon and collect the scattered signal is a scattering-type near-field microscopy (s-SNOM), as is shown in. Fig. 6. The working principle is similar to the lightning rod effect; the basic idea is to illuminate a sharp tip of an atomic force microscope (AFM) with infrared light. The tip in turn acts like a dipole emitter which spans momenta extending up to a few times of $1/a$ at IR frequency ($\sim 10.6\mu$m), where $a \approx 20$nm is the size of the AFM tip. This enables matching of the frequency and the wave-vector to excite graphene plasmons. The spatial resolution of the near field $d \sim z/2$ where z is the distance from the tip to the sample. The distant between the tip and the sample can be as close as 20nm allowing the spatial resolution to be as good as 10nm (in the condition that it does excess the range of few times 1/a) Comparing to the diffraction limit of 10.6μm in near-IR, the resolution is over thousand fold better. This is a remarkable idea that improves the spatial resolution by thousand fold without changing the energy of the photon. This principle can be, in tehory, applied to all wavelength regime which will enable the study of not just plasmons but also light matter interaction in various energy scale and wave-vector.

3.2   Experiments and references

In recent years, graphene has attracted tremendous attention in condense matter physics because of its exotic electronic property. Graphene is a mono-layer sheet of carbon atoms arranged in hexagonal configuration. As layers of graphene stack together, graphite is formed and the interaction between graphene sheets is weak van der Waal force, which makes it easy to separate via mechanical exfoliation. Single layer graphene has electronic structures completely different from graphite when set free from van der Waal inter-action. The band structure of graphene near fermi point has linear energy momentum dispersion. This implies that the effective mass of the free charge carriers inside graphene is zero. Thus, the carriers will exhibit extraordinary transport properties, for example very high mobility which cannot be com-peted in ordinary materials. Moreover, the wave function of this massless electron is governed by Diracs relativistic wave equation which usually is used to describe particles in high energy scale. This new platform allows us to study high energy scale behavior of Dirac electrons in low energy scale
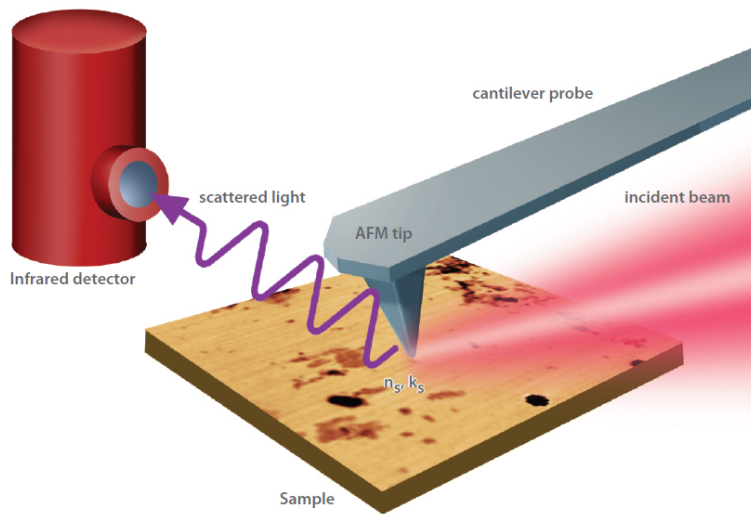
Figure 6: Schematic drawing to illustrate the basic idea of s-SNOM. A ray of near-IR laser beam is illuminated on the tip of an atomic force microscopy which polarizes the tip into a dipole. The tip in turns emits photon in IR frequency confined in a distant of a few times $1/a$ (where $a \sim 20$nm is the size of the tip). The scattered light from the sample is then collected and demodulated to feed back information about the sample. Picture is obtained from anasysinstrucments.

and in an environment filled with abundant amount of tools and methods rather than trying to observe it in an particle accelerator.

This new platform has abundant amount of applications and unexplored physics inside. One can study the intrinsic property of Dirac electrons by suspending it in air and thus eliminating any van der Waal interaction on graphene. One can also place superconductor, magnetic or electric dielectrics on top to construct various heterostructure to study collective behavior of Dirac electrons. Tremendous progresses have been obtained in graphene but there are still many dark corners waiting to receive a ray of light. Recently, graphene has gotten a lot of attention from near-IR side because the excitation energy scale of near-IR is in the regime of the size of Dirac cone, which allows one to excite Dirac electrons from valance band across the Dirac point to conduction band and relax via the linear energy-momentum dispersion. Together with its high carrier mobility and small scattering factor γ of massless Dirac electron, all these features make graphene appear as an excellent candidate for plasmonics, despising the fact that graphene has much lower carrier concentration than ordinary metal. Many theoretical calculations and predictions, along with some experimentally verified results, have shown the promising future of graphene plasmonic application. Among them, there are a few results relevant to our research and shall be pointed out here as follows.

3.2.1 Gate tuning of graphene/SiO2 plasmons in near-IR [11]

One of the early and influential paper on graphene plasmon was done by Z. Fei in Basovs group in 2012. He observed SPPs on the physical edge of graphene and around defects. There are a few remarks they made and we will point them out here as reference to our experiment.

The apparatus they use to take these data was also s-SNOM and in the same near-IR regime as our experiment. They had observed several important features of graphene plasmon which are relevant to our research to compare and understand our system. First of all, graphene plasmon can be observed in this frequency regime without the need of very high carrier concentration. As can be seen from the calculation in chapter 2 where the calculation is based on a Drude metal of carriers of the order of 10^{23}/cc. Graphene typically has carrier concentration of the order of $10^{12}\mathrm{cm}^{-2}$. To compare, one should convert the 3D carrier concentration to 2D, assuming 1μm thickness Drude metal (1μm is reasonably thick enough to be called 3D). Then the 2D carrier concentration can be estimated roughly in the
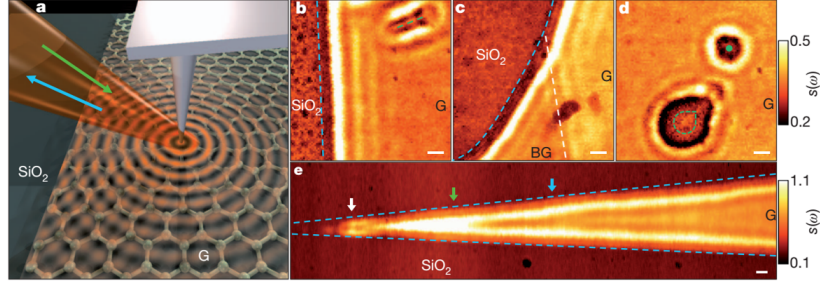
Figure 1 | Infrared nano-imaging experiment and results. a, Diagram of an infrared nano-imaging experiment at the surface of graphene (G) on SiO$_2$. Green and blue arrows display the directions of incident and back-scattered light, respectively. Concentric red circles illustrate plasmon waves launched by the illuminated tip. **b–e,** Images of infrared amplitude s ($\omega = 892\,cm^{-1}$) defined in the text taken at zero gate voltage. These images show a characteristic interference pattern close to graphene edges (blue dashed lines) and defects (green dashed lines and green dot), and at the boundary between single (G) and bilayer (BG) graphene (white dashed line). Additional features marked with arrows in **e** are analysed in refs 27 and 30. Locations of boundaries and defects were determined from AFM topography taken simultaneously with the near-field data. Scale bars, 100 nm. All data were acquired at ambient conditions.

Figure 7: Gate tuning of graphene/SiO2 plasmons in near-IR [11]. As Basov et. al. mentioned in the caption, the graphene is on SiO$_2$ substrate and they launched plasmon from AFM tip using wavelength of $\sim 10\mu$m. As a plasmon bounces back from physical boundary of graphene/air interface, it creates interference patterns from both edges, see e. Two important remarks we should make here are 1. Plasmons can already be observed in regular quality condition, in the sense that the fermi level is sitting not too far from the Dirac point, which implies that the carrier concentration is relatively low. The bottom interface is SiO$_2$, which interacts with graphene via van der Waal interaction and has many defects/residues, which can be seen from the non-uniform dark spots on the SiO$_2$.These factor will contribute to greatly lowering graphenes electronic properties such as mobility; 2. The defect they observed was acting like a physical boundary that is dark (nonconductive) and was preventing plasmon from propagating inside. These observations will be further compared with our experiment and results as reference.

order of 10^{17}cm^{-2}, which is still many order higher than that of graphene. As we have discussed about, the relation between longitudinal propagation length and carrier concentration in equation (16), graphene will have much shorter propagation length scale compared to a good metal like gold and silver. This can be seen from Basovs data from b-e in Fig. 7. The plasmon fringes are barely visible as short as the third peak. However, on other hand, it is surprising (if we purely treat graphene as a poor metal) to even see plasmon on this order of carrier concentration. The advantage of graphene as a plasmon platform is its unparalleled mobility and low loss (small scattering factor). Moreover, the quality of the graphene matters since it will greatly affect electronic properties such as mobility of Dirac electrons.

The plasmon wavelength is roughly 100nm from their data, as is shown in Fig. 8, when the fermi level is around the Dirac point. Another snap information from their paper is that they found the scattering factor γ=0.135 by fitting their data. This number is not very low nor high, compare to $\sim$0.2 of silver. However, the quality of the graphene sample they measured is not in its full potential. As one can observe from Figure 7, the SiO_2 has many dark spot in the near field indicating defects or residues in which the graphene is sitting on. As we had mentioned briefly before, any interaction on graphene will change its property drastically because the band structure is not protected by symmetry that protects it against defects or EM interactions. Therefore, the interface between SiO_2 and graphene will provide a drag back on the intrinsic Dirac electrons one would expect. Graphene is also likely to be doped with water from the air and degrade quickly, through it might be a good sign for plasmon because of higher carrier concentration naturally coming from doping. In our experiment of studying defect and doping of graphene with O_3, we have the same setup with graphene sitting on a SiO_2 and in contact with air. Even though we have the ability of suspending the graphene but for a cost of small tunable gate voltage and will have chemical resides such as poly methyl methacrylate (PMMA), we chose to place graphene on SiO_2 for a different reason which will be mentioned in our experiment session. Another observation of their data that is relevant to our study is that the defect they observed with plasmonic fringes surrounding it is a hard boundary and is darker inside the defect. Plasmon cannot penetrate or propagate into the defect regime will be shown as the data above.

The way s-SNOM register the plasmon oscillations is shown in Fig. 9. As the AFM tip scan near the physical boundary of the graphene it creates
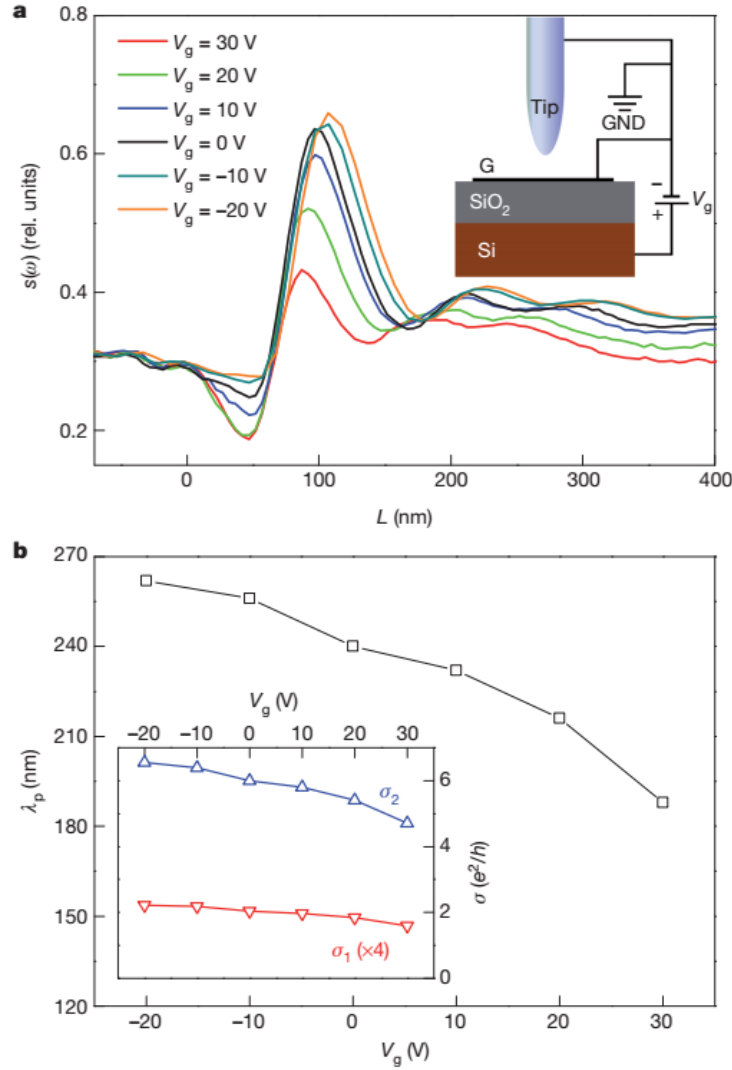
Figure 3 | Electrostatically tunable plasmons in back-gated graphene.
a, Line profiles of $s(\omega)$ perpendicular to the graphene edge at various gate voltages, V_g. Inset, our gate bias set-up. Both the metalized tip and graphene are at ground (GND) potential. **b**, Gate-dependent plasmon wavelength λ_p. Inset, σ_1 and σ_2 of graphene at various gate voltages, estimated from λ_p and γ_p, as described in the text. These conductivity data show directly that the infrared response of graphene is predominantly reactive, $\sigma_2 \gg \sigma_1$, thus fulfilling an essential precondition for excitation of plasmons.

Figure 8: Data from [11]. As was mentioned in their caption that they see a correspondent between carrier concentration (by turning gate voltage) and plasmon wavelength as expected but the advantage over a good metal such as gold and silver is that their plasmon wavelength is not noticeable by tuning gate voltage due to the abundant amount of free carriers they already have.

18
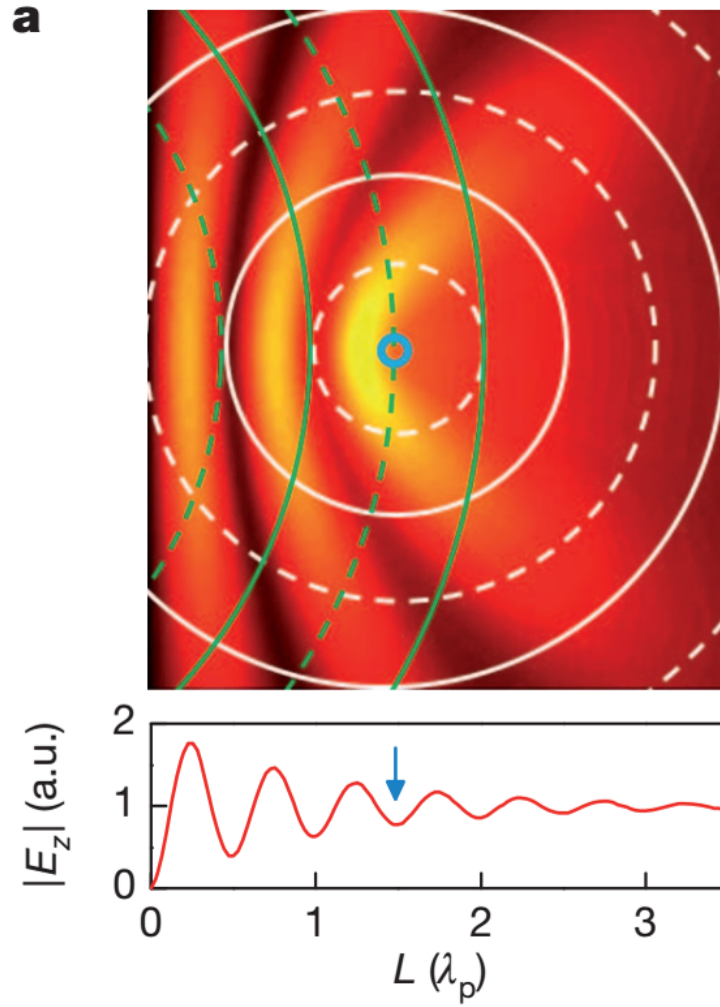
Figure 9: Interference pattern of plasmons launched from the AFM tip (in the center) with the reflected plasmon wave from the physical boundary (on the left). The bright fringes are the near field signal registered on the data. The period of the plasmon wavelength should be of the oscillation observed in the data plot.

19

interference pattern of wave launched from the tip and waves reflected from the physical boundary. The plasmon oscillation is registered as bright fringes shown in the figure and the plasmon wavelength λ_p should be 2 times the wavelength observed in the data. In this case the distance between plasmon fringes is roughly 100nm which implies the real plasmon wavelength should be ∼200nm which is also the typical graphene plasmon wavelength.

Basovs group recently published a follow up experiment on graphene plasmon in collaborating with Columbias engineering group which shows enhanced plasmon fringes from an extraordinary high quality graphene sample done by mechanically, chemical free stacking of hexagonal Boron Nitride (hBN) sandwiched graphene and is bubble free, wrinkle free. The basic idea is that the lattice structure of hBN matches that of the graphene very well and hBN exhibit plasmon oscillation of phonons in the near-IR regime and with similar plasmon wavelength making it a natural resonator/enhancer to boost graphene plasmon. Moreover, the losses in graphene hBN sandwich is greatly reduced because of atomic flat hBN creates a clean interface for graphene on top and bottom. The graphene hBN sandwich has shown an improvement of mobility of orders higher than graphene on SiO_2. We will skip the details here but the main remark that it has shown great promising results of the potential of graphene in plasmonic.

One of the advantage of the graphene from ordinary good metals in plasmonic application is plasmon with low carrier concentration. As we had repeatedly shown from calculation and experimental data, carrier concentration is one of the most crucial factor in plasmonic and thus, will be good to be able to manipulate it. The carrier concentration of graphene can be changed by gating or doping and the ratio of the change is significant which in turns affect the plasmon wavelength and propagation distance. The manipulation of carrier concentration does not ends here, one can create a p-n junction or preferably, a switch (field transistor), that turns on/off the plasmon or to confine the plasmon into a small regime are all made possible with the freedom on effective carrier concentration manipulation. This will require the experimental study of p-n junction of graphene plasmon which is part of our project and is still ongoing. We should first review a theory calculation of how p-n junction affects graphene plasmons propagation.

3.2.2 Guided plasmons in graphene p-n junctions [5]

In Mishchenkos theory calculation of a propagation of graphene plasmon across a p-n junction. In the calculation, they considered two type of p-n junction, one is field induced created by electron and hole puddles on the graphene by dopant or other means. The other one is gate induced by metallic gating. In here, we will focus mainly on the latter case because it can be relatively easy to achieved and with more control of the size and height of the potential wall.

When a graphene plasmon travel across a p-n junction, it can bounds back or transmitted or both, thus forming observable plasmonic fringes. The crucial criteria in the junction is the strength of the gating field and also the sharpness of the junction. As shown in the paper, the dispersion relation of graphene plasmon reflected from the junction in the case of the width of the junction is larger than the wavelength of the plasmon:

$$\omega_0^2(q) = \Gamma^2(3/4)\frac{4e^2vd}{\pi\hbar l_E}q^2\ln(1/qd),\tag{23}$$

where q is the wavelength of the plasmon and $2d$ is width of the p-n junction. It is important to note that the width of the junction should be larger than 200nm (typical wavelength of the graphene plasmon).

To conclude this chapter, we should briefly summarize our experiment and their goals. The main study in this paper will be focusing on plasmon of defects and doping on graphene by UV ozone. UV ozone creates O_3 ions which will attach on the surface of the graphene with different bonding strength depending on the UV ozone time. By controlling the radiation time (or oxygen level by placing the sample in a seal chamber), the amount of defects and charge induced on the graphene can be controlled. In small amount of time (< 3mins), the damaging on graphene is not noticeable (more careful study needed to justify and confirm this). The non-uniform carrier induced by doping are observed by plasmon fringes distributed randomly in the interior of the graphene. The removal of oxygen dopant by annealing are preliminary studied. It is important to note that the topography of the sample has little to no change while the near-IR signal change drastically. The possibility of topography effect and other issues are addressed.

Another project is to study defects on graphene induced by annealing in air for high temperature (> 300C). The defect forms soft boundary in which the plasmon can travel inside and forms modes. As we increase the annealing
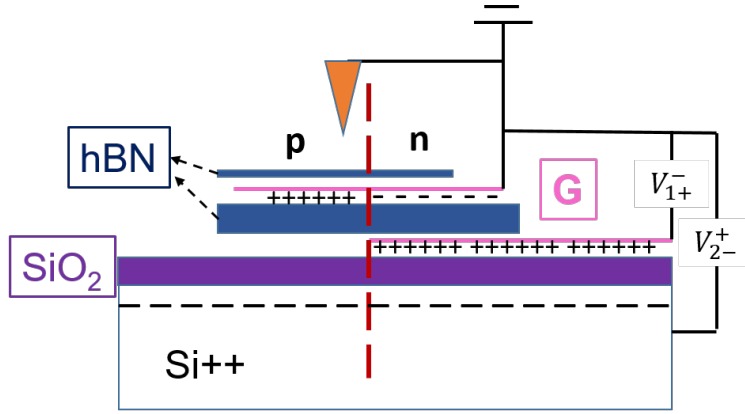
Figure 10: Schematic set up of p-n junction device. From the bottom Si++ doped SiO_2 substrate to top; the layers in order are back gating graphene (< 5nm), hBN ($\sim 20 - 100$nm), monolayer/bilayer graphene and finally a covering top hBN (< 10nm). The relative position of each part are drawn as shown in side view, the bottom graphene used as gating is shifted to cover only partially the top monolayer/bilayer graphene so that when double voltage source is applied, an gradient of p-n junction is induced on the sample. The AFM tip and the monolay/bilayer graphene is grounded in order to eliminate charging effect between them. Red dash line is the boundary of the gate induced p-n junction.

temperature, the defect eventually becomes a hard boundary in which the plasmon are reflected back completely.

As we mentioned earlier, we also pursue the graphene plasmon propagating across a p-n junction. Heterostructure of hBN sandwiched graphene with graphene back gate and overall substrate back gate structure are fabricated with mechanical exfoliation and dry mechanical stacking. The schematic set up is shown on Fig. 11. This device is capable of gating the sandwiched graphene with subtract and also a flake of graphene below and covered partially the graphene sandwich to create a field induced p-n junction with various strength. The junction width is d is proportional to the bottom hBN which has size can easily vary from few nm to hundreds of nm. However, no noticeable plasmon fringes around the boundary are observed among over 5 selected samples with least amount of bubble and wrinkles. Possible causes will be mentioned. Another parallel project similar to the structure in Fig.

11 is to study the surface plasmon resonant of two graphene sheets on top of each other with vary distant. Because the surface plasmon travels not just in the metal but also in the dielectric with amplitude decaying exponentially as shown in equation (20). It turns in order to see strong resonant condition, the distant between two graphene sheet should be very close (10-100nm).

Chapter 4 Sample Fabrication

There are multiple interests in plasmon study not limited to purely graphene but also other materials (e.g. black phosphorus of less than few layer thickness) to create heterostructure to study various effects. For each project, the sample structure and requirement vary a lot. But here we will be discussing only our most fruitful results and the preparation and fabrication of corresponding samples.

4.1 Graphene plasmon study of defects and oxygen doping

Defects and doping are fundamentally important in applications and also understanding of charge carriers interactions inside the material. In our experiment, we generate ozone on the surface of graphene with UV light, which the activated oxygen will interact with the graphene sheet and remain there. The effect of oxygen bonds, in turns, donates free charge carriers locally. There has been a lot of interest in various field trying to attach various ions on the surface of the monolayer carbon sheet to change electronic properties of free carriers in the graphene or induce a magnetic moment. However, there wasnt many success examples. Finding such an element to attach on the graphene chemically stable is difficult. The choices are limited and so far, the most successful example is to attach hydrogen atom on graphene which in turns creates a local magnetic moment in atomic scale. Even though there are still stability issues up to room temperature. It has the potential of creating atomic memory array to store information. It can increase the density of information storage tremendously. [**?**] Compared with our experiment, even though oxygen doping of graphene cannot be used in making memory, it is fundamentally useful in manipulating graphene plasmons via doping or application wise such as pattern graphene and selectively doping it. One advantage of this doping is the low energy scale, where a graphene sheet can be doped directly in room temperature with chemical stability and damage ranged from small to negligible. It is also worthwhile to mention that the control of the doping level can be very finely controlled. One can, in theory, adjust the oxygen level or lower the temperature around the sample and tune the intensity of the UV light to achieve desired doping rate and uniformness.

The graphene sample to study the UV ozone doping effect and annealing defect with graphene plasmon should be as clean as possible because one can always argue the source of defects/dopant being anywhere during the complex

fabrication process (i.e. residues on the sample from PMMA, photoresist or even from solvents). Therefore, it is important to eliminate any sources of dopant studying the UV ozone doping. The same applies to defect from graphene annealing and in fact the sample is the same for these two studies.

A blank 300nm SiO_2Si substrate is first submerged in acetone solvent and heated up to 80C for 15mins and then is sonicated sequentially in submerged solvent of acetone, IPA and distilled water for 15mins each. The substrate is then etched in oxygen plasma for one and half minutes and then baked for 400C for 10min. One can achieve a cleaner result if adding in process a piranha etching for a few minutes. This whole process of sample preparation can eliminate most organic residue and dirt on the subtract. However, native defect of SiO_2 cannot be removed. We can exfoliate graphene flakes onto the substrate via mechanical exfoliation and the surface of the graphene is freshly peeled from natural graphite obtained from Germany and is atomically flat. So defects that are affecting the backside of graphene are reference images/data which will be compared with the condition after the UV ozone/annealing treatment. It is the relative change before and after UV ozone/annealing that we are interested in.

4.2 Graphene hBN heterostructure for plasmon study of p-n junction and resonant

In this study, the sample requirement is very strict and hard to achieve without the use of dry mechanical stacking method. First of all, we are interested in studying graphene plasmon propagating through a p-n junction where the reflection and transmission are very small making weak interference patterns with the plasmon wave launched from the AFM tip. And even with physical boundary, the visible plasmon fringes are only two or three on graphene SiO_2 structure. So it is natural to first improve the quality of graphene, and thus increase the amplitude and propagation length of the plasmon in order to observe any tiny plasmon fringes on the junction. As we had mentioned in the end of section 3.1, one can improve the visibility of graphene plasmon fringes by coupling it with the phonon plasmon from hBN. In order to improve the plasmon signal from across the junction, and for simplicity, we designed a heterostructure as schematically shown in Fig. 11.

However, there are tradeoffs from making such devices, because the resolution and field penetration depth of s-SNOM is only a few times $1/a$ where

a is the tip size ($\sim$ 20nm), and the resolution of the near field is limited by the distant from the tip to the sample. It turns out that the thickness of the top hBN should be 10nm or less, otherwise the near-IR wave launched form the AFM tip cannot launch graphene plasmon. The thickness of the bottom graphene (as gating electrode) and the insulating hBN should also be small, in orders of $\sim$ 10nm and $\sim$ 100nm respectively. Reasons are the following. Firstly the bottom gating electrode (graphite) should be atomically flat and thin otherwise any roughness will appear on the graphene we want to study and will affect the sharpness of the gating boundary. The hBN between the graphene and graphite should be relatively thin for effective gating from the Si++ doped substrate on the bottom. The distant between substrate backgate to the graphene sample is the thickness of 300nm SiO_2 and the thickness of the hBN between the graphene and graphite. However, according to the theory calculation of graphene plasmon across p-n junction in the paper mentioned in section 3.2.2, the width of the junction should be larger than the wavelength of the graphene plasmon ($\sim$ 200nm) in order to see reflective interference. In our setup, the width of the junction can be think of a few times the thickness of the bottom hBN and the actual coefficient is to be determined. Therefore, multiple devices with various thickness of hBN ranging from 10s to 100s of nm should be investigated.

Another important thing to consider is the cleanness of each layer. Any residue or dirt on the layer will form bubble during mechanical stacking. Therefore, using wet mechanical stacking with polymer such as methyl methacrylate (MMA) will leave residues after removal with acetone and not produce a high quality device. A wet mechanical stacking is to use a uniform layer of polymer such as MMA and mechanically exfoliate the desired van der Waal crystal onto this polymer and then place the desired flake on the polymer to a targeted spot on the substrate. After heating up and melting the polymer, the polymer and the flake will stick on the substrate. Then the substrate is dipped in acetone or resist remover solvent to remove the MMA. This process can be repeated with another flake in the same spot to make a stack. However, the removal of MMA with solvent will always leave residues (nano-size) as studied with high resolution AFM and is not easy to remove completely. So typically other methods such as vacuum baking in high temperature is needed for better removal of the residue. A dry stacking is similar but with a different polymer that does not require to melt because of more adhesive surface with the crystal via stronger van der Waal force. We will discuss the process step by step in the following section. Therefore, to make a bubble

free stack, one might need an absolute clean and dry environment such a glovebox with purely nitrogen gas inside. I first came to my thesis advisor, Prof. Du's lab starting from the beginning of this semester, there was only wet mechanical stacking method available and to achieve the goal of my projects, a dry method was developed and I had overcame various technical difficulties that enriched my experiences.

In this part, we will discuss in detail how the structure of Fig. 11 was fabricated. An overview of the basic idea is that we will spin coat a thin layer of highly adhesive polymer (but no glue or any liquid on the surface of the polymer), called polypropylene carbonate (ppc), on a soft polydimethylsiloxane (PDMS). Both polymer are highly transparent. Then we mechanically exfoliate hBN onto a clean substrate and find, with optical microscope, the flake you desire. We first pick up the hBN flake with ppc (hBN stick better on ppc than the substrate). Then we exfoliate a second flake, i.e. graphene, onto a clean substrate and we pick it up with the hBN that sticks on the ppc. The hBN flake is atomically flat and so can easily pick up any crystal via van der Waal force from the less adhesive substrate. And this process can be repeated, in theory, to make any number of layer of flakes. And because the flakes are freshly peeled onto the clean substrate, there flake will be clean. And note that this process does not require the use of solvent until at the end, you melt the stack along with the ppc onto the substrate and it is the cleanness within the stack that matters. The residue on top of the insulating hBN will not affect the property of the sample within the stack. One can in theory replace hBN with other van der Waal materials to create many interesting heterostructure and the combination can be infinite making it a valuable method to make clean and complicated devices to study in various direction. For example, one can sandwich ferromagnetic dielectric on topological insulators (TIs) to study magneto interfacial effect to the spin-momentum locked Dirac electrons on the surface of the TIs.

4.2.1   Substrate preparation

The whole process starts with cleaning substrates. A recycled 300nm SiO_2/Si substrate (previously mechanically exfoliated crystals on the substrate) is first submerged in acetone solvent and heated up to 80C for 15mins then is sonicated sequentially in submerged solvent of acetone, IPA and distilled water for 15mins each. The substrate is then baked for 400C for 10min.
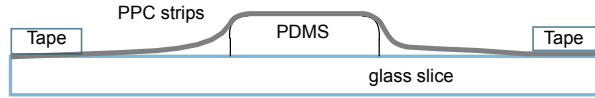
Figure 11: Schematic sturcture of a ppc stamp. The PDMS is placed on a glass slice and ppc is spin coated on a plastic sheet and scissor into strips is then taped on top of PDMS carefully to eliminate any bubbles.

4.2.2 ppc stamp preparation

ppc crystals are dissolved in anisole by weight (15% of ppc). The solvent is placed in stirrer and stirred overnight. PDMS is prepared on glass breaker (to ensure flatness) with mixing ratio of part a and b as recommended by manufacture. The PDMS liquid is then leveled and placed in a desiccator pump continuously for 2 hours to purge any bubbles within (to ensure better transparency and flatness). The PDMS is then heated to 60C to cure further and is ready to use. The disk of PDMS then placed in oxygen plasma etching for one and half minutes to make it overall flatter but also locally rough. This can improve the adhesion between the ppc and PDMS. Then a small square ($\sim 2\text{mm}^2$) are cut form PDMS dish and place on a clean glass slide. There are two options from this point and both works. One is to spin coat ppc directly on the PDMS which however, sometimes the ppc is not uniform due to the geometry of the PDMS and the adhesion between them is still low. I choose a different route which works and easier. I spin coat ppc on a sheet of clear plastic sheet that can be found from staple or other places. I believe any clear plastic sheet that is also soft (not too thick) will work and the adhesion between ppc and the plastic sheet is much higher than that of PDMS. Second reason I chose plastic sheet is because I spin coat a large area of plastic sheet fixed on a larger glass slide. The plastic sheet is flat and has huge area which makes spin coating much more uniform in the center region than on the small PDMS. The spin coat speed is 3000rpm with acceleration roughly 1000rpm/sec. The plastic sheet is then baked with 80C for 5mins or in case of ppc/PDMS, 100C for 2mins. I then scissor the plastic sheet into strips and use only the center area of each strips. The stripe of plastic sheet with ppc coated is then placed carefully on top of the PDMS/glass-slide and tape both side of the stripe to fix it. The ppc stamp is then complete and can be used to pick up crystals. The schematic structure is shown in Fig. 12.

28
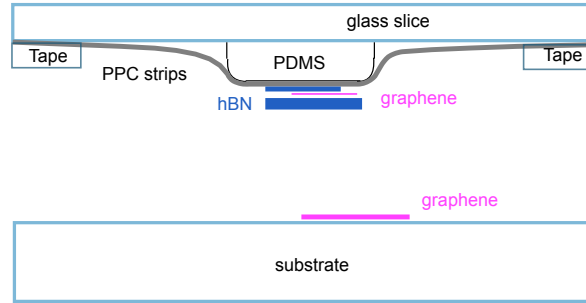
Figure 12: Schematic structure of placing a graphene sandwich on a graphene sitting on a substrate. Typical size of the flake are order of 10um and the aiming accuracy will greatly depend on the visibility of the crystal and mechanical control of the stage. The error of aiming is roughly 2-3um which sometimes is matters as the structure of the junction can be as small as $\sim 3\mu$m. Therefore it is important to have highly transparent ppc stamp.

It is important to keep ppc in clean environment because it likes to attract any dirt from air.

4.2.3 Stacking process

As we have mention briefly the basic idea and process of stacking, fresh crystal flakes of hBN and graphene will first be exfoliated with blue tape onto substrate. Fig. 13 shows a schematic structure of stack. Firstly we pressed down the ppc stamp onto the desire hBN flake then heated up the substrate to around ~ 60C then let it cool down immediately (sometimes the temperature might need to be higher in order to pick up the flake). This process will increase the adhesive between the ppc and the hBN flake by stretching and thus, release bubbles and increase their contact area. It is best to operate the ppc stamp in cool temperature because the ppc polymer will become soft as temperature increasing and become easy to tear off during releasing process. After picking up the initial hBN flake, the heating process is unnecessary because the hBN is atomically flat and has a stronger van der Waal attraction than ppc to graphene. If heated up, ppc will stretch the hBN which might result in wrinkles or cracks. And this process shall be repeated until we have on ppc from bottom to top, hBN, graphene, hBN and

29

Figure 13: Optical image of a hBN graphene heterostructure as the schematic set up in Fig. 11. The graphene sandwiched by hBN is transparent but the location is extended out to the yellow colored electrode extended on top of the hBN (light blue) and the top hBN (slightly yellowish). Note that the top hBN is also very transparent due to its thinness ($\sim$ 5nm) the bottom graphite (purple) is the bottom gate crossing partially the sandwiched graphene. Note that there is a fork like underneath the graphene sandwich.

graphene. And at the last stamp on the graphene, the substrate is heated up to over 120C to melt the ppc and leave the whole stack on the substrate. The substrate is then submerged in acetone for 30mins to remove the ppc. The electrical contact of the sample will be made with E-beam lithography using PMMA A4 and with metal Cr/Pd. Fig. 14 is an optical image of such stack. The graphene sandwiched by hBN is transparent but the location is extended out to the yellow colored electrode extended on top of the hBN (light blue) and the top hBN (slightly yellowish). Note that the top hBN is also very transparent due to its thinness ($\sim$ 5nm) the bottom graphite (purple) is the bottom gate crossing partially the sandwiched graphene. Note that there is a fork like underneath the graphene sandwich.

Chapter 5   Results and Analysis

Even though mentioned earlier, the results will be presented from the most fruitful to the least, it is more natural to start from the original goal which is to guide graphene plasmon with a p-n junction, because the defect study was a side result.

5.1   Graphene plasmon and p-n junction

The optical image on Fig. 14 has the heterostructure as the schematic drawing in Fig. 11. The monolayer carbon sheet between the hBN sandwich is invisible due to the refraction index mismatch on this setup. One thing to note in this set up is that the bottom graphite (as back-gate) is a fork shape underneath the graphene sandwich whose original purpose is to create a p-n-p potential well to enhance the interference of the graphene plasmon (if there is any) between the walls and thus, increase the signal.

The near field and AFM topography image of the hBN sandwiched graphene is shown in Fig. 15. The location of the scan area is roughly indicated in the square box in the optical image. In the near field image, two bright graphene strips not covered by hBN can be seen and they are multilayers. The rest of the graphene is monolayer/bilayer connects bright strips and extend into the right side where the boundary of top hBN can be seen. The AFM image (the right one in Fig. 15) shows bubbles with various sizes distributed across the surface. There are many smaller bubbles distributed across the top hBN and less on the bottom hBN (the left one in Fig. 15). This is because the top hBN is thin ($\sim$ 5nm) and thus, much softer than the bottom hBN and easier to trap bubbles. The graphene between the hBN is too thin to be seen in the AFM image ($\sim$ 0.5nm) but can be seen relatively easy in the near field because it is conductive showing up in color (either dark or bright) while the hBN is insulating and thus, lesser respond from near field.

The result of applying gate voltage is shown in Fig. 16 to 17. A high contrast in color of each area injected with different carrier types can be visually seen. Between bright and dark area, a sharp boundary can be seen.

There are a few things needed to be considered to create a real p-n junction. So far, the right picture in Fig. 16 can only claim, at most, as a potential wall as can be seen from the contrast. This is because that both the dark and bright area of the graphene can still have their carriers being the same carrier type. The contrast of different color between the regions tells only the

31
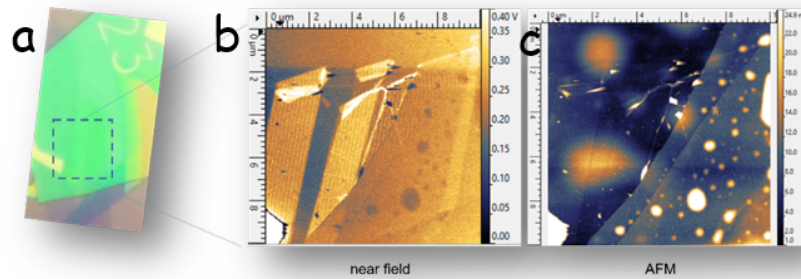
Figure 14: Near field and AFM topography image of the hBN sandwiched graphene. The location of the scan area is roughly indicated in the square box in the optical image. In the near field image, two bright graphene strips not covered by hBN can be seen and they are multilayers. The rest of the graphene is monolayer/bilayer connects bright strips and extend into the right side where the boundary of top hBN can be seen. The AFM image shows bubbles with various sizes are distribute across the surface.(right) There are many smaller bubble distribute across the top hBN and less on the bottom hBN (left). This is because the top hBN is thin ($\sim$5nm) and thus, much softer, than the bottom hBN and easier to trap bubbles. The graphene between the hBN is too thin to be seen in the AFM image ($\sim$0.5nm) but can be seen relatively easy in the near field because it is conductive show up in color (either dark or bright) while the hBN is insulating and thus, more transparent in near field.

Zero biased

$V1 = -10, \qquad V2 = 60$
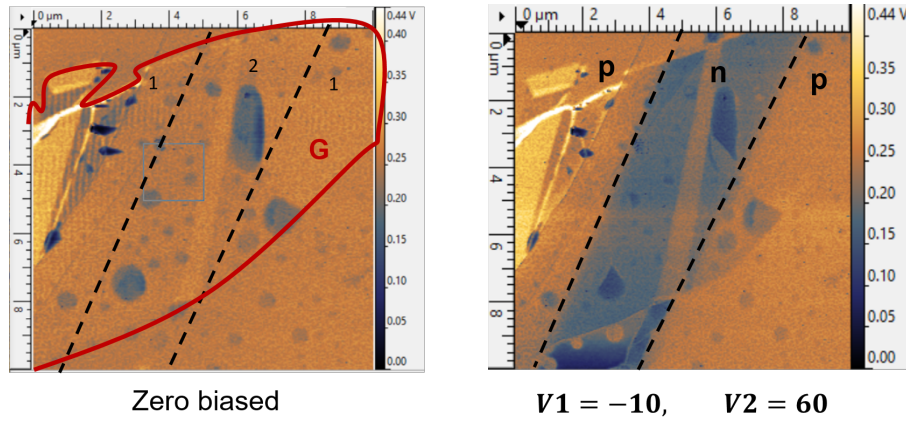
Figure 15: Gate tuning of p-n junction. The circuit connection is shown in the schematic drawing in Fig. 11, the black dash lines indicates the junction. The red boundary is the location of the sandwiched graphene (left). The purple puddles are the bubbles. The picture on the left is before applying gate voltage and the picture on the right has gate voltage of V1=-10V and V2=60V. The boundary of the graphite underneath can be seen after applying a gate voltage and the contrast different are indication of change of carrier concentrations of both graphene sheet and forming a potential different at boundary of the black dash line. The sign p and n on each part are symbol of either injecting electrons (n) or holes (p) carrier.
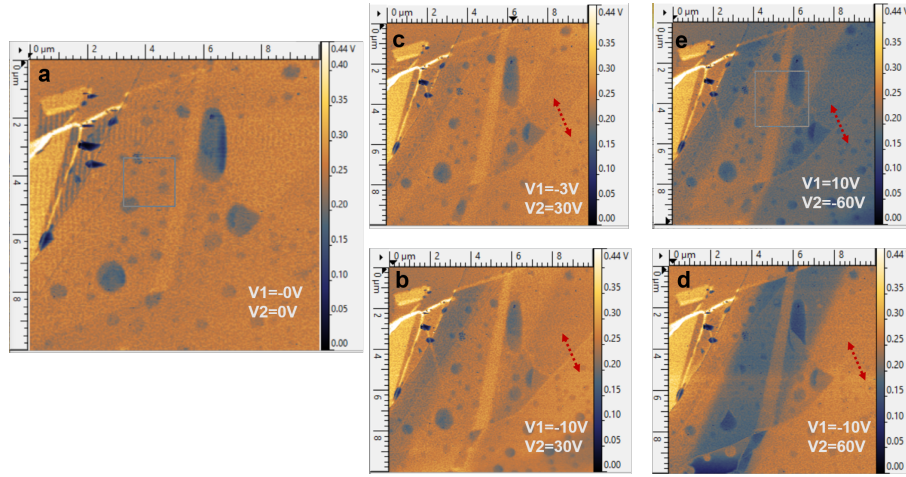
Figure 16: Same area near field scan of p-n junction device with various gating voltage of V1 and V2. The circuit is shown in Fig. 11.

different, in area, the carrier concentration. What Fig. 17 has is a collection of near field scan of same areas with different applied voltage source V1 and V2. The main result is, there is no graphene plasmon fringes found across the boundary. There are a few possibility that might be able to explain this result.

First of all, there might be no p-n junction across the boundary after all. To understand whats going on, we should analysis the data in Fig. 17. Part a of the figure is zero biased near field image and the boundary of the junction is invisible since the carrier are uniform across the graphene. The graphene channel is still visible because the Fermi level of it is not right at the Dirac point. From experiences, almost all high quality graphene has their Fermi level initially close to the Dirac point and will be doped by water or various solvent from the environment that donate holes to the graphene and making it p-type. For example, in Fig. 8, the sample measured in Basov's paper, shows a gate voltage vs conductivity plot and implies the sample is p type at zero bias. If we assume both of our graphene and graphite is initially p type then the voltage applied in part b of the figure will push fermi level of top graphene up and pushes (Fermi level of) the bottom graphene down. This implies the bottom graphene will gain more holes and become more conductive while top graphene become less. In turns of near field signal this

34

will mean brighter and darker respectively. This corresponds to the behavior of part b, the top graphene becomes darken as the bottom graphene starts to light up. The relative contrast behavior are indicated as red arrow on the figure. Part c of the figure, the top graphene receive even more electrons and became even darker indicating the Fermi level has not pass through the Dirac point but still approaching it. Part d of the figure, the bottom graphene receives even more holes and light up further creating a sharper contrast between the areas of different potential. At figure e the polar are reversed and the color are flipped. The first view of last switch seems reasonable for a p-n junction but however is not true in near field. The near field measure the carrier concentration and if the last flip pushes the fermi level of the bottom graphene to other side and to graphene deeper into p type then we should see an increase in brightness for top graphene while bottom graphene might become darker. The top graphene should reduce the darkness of the bottom graphene but it is not the case (see the red dash line in part e). Therefore, this implies even after the flip, both graphene are still sitting in same carrier type.

Another thing needed to be consider is the band structure of graphite. It is a semiconductor with a small band gap (for multilayer). The change in contrast respect to the change in voltage might not be visible when across the band gap. And the carrier injected into the top graphene should be at much as possible because the visibility of plasmon fringe is directly proportional to the carrier of the graphene sheet, which, we have it inverted and our top graphene seems to be gated closer to the Dirac point.

Lastly, the thickness of the hBN and the width of the boundary might be crucial because they will directly affect the effectiveness of the gating and sharpness of the p-n junction. Note that the junction does not necessary needed to be thin, it might be better to have a junction width d SPP 200nm. It might be better to pattern an graphene strip with various size to create a p-n junction without using the substrate as gating electro and without top hBN (to eliminate bubbles and wrinkles).

While trying to make the surface of our device cleaner and get rid of bubbles with annealing and UV ozone, we discovered IR plasmons are excellent indicators for defects and oxygen dopings.

35
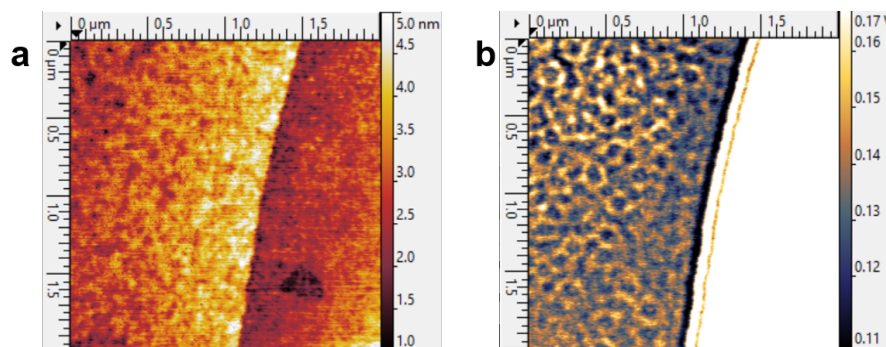
Figure 17: Graphene plasmon in the interior after sequentially 2min and 3minute of UV ozone (for time treatment less than 2 minutes the change is small). a. AFM image of graphene and SiO_2, the surface is uniform, no damage is observed in this scale. b. near field image of graphene shows plasmon fringes distribute uniformly the interior of the graphene.

5.2 Graphene charge doping with UV ozone and defects

Near field study of graphene plasmon require very high quality sample as we had emphasized from previous session, therefore, it is natural to try annealing or UV ozone to improve the sample quality. We found that, UV ozone can be used to dope graphene and introduce graphene plasmon on open surface, not limited by physical boundaries. See Fig. 18.

The UV ozone emits UV frequency that matches the resonant frequency of the oxygen bond and thus, breaking it and form O_3 ion. This ion is non-stable and will dissipate over time and reduce back to O_2 as it loses energy. The O_3 ion is very reactive and will oxidize metal or break organic bonds. Therefore, it is usually used as a powerful organic etcher. Typically, we use it in lab to remove organic residues on graphene and it does little to no damage to graphene for time less than few minutes. If the graphene is exposed in ozone for too long, it will eventually oxidize the graphene. The O_3 ion also can attach to the surface of substrate or graphene because its an active ion. Normally one can bake the sample in high temperature ($\sim$200C) to remove the O_3.

We will first study the effect of UV ozone time for longer time (5mins), then try annealing in sequent of increase temperature, to reduce the oxygen ion and return the sample back to the original condition. Then we will study

36
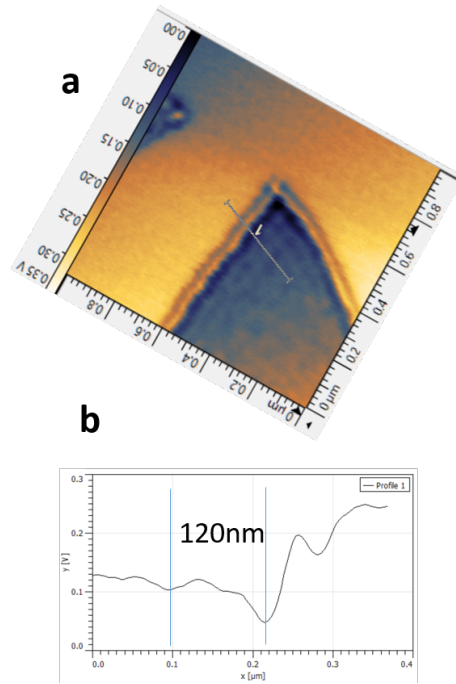
Figure 18: Near field image of intrinsic graphene on SiO_2.The wavelength of graphene plasmon is two times the fringes distant which is about 240nm. Consistent with theory and reported value (see Fig. 8).

the effect of UV ozone time by sequentially increase the treatment time.

We should first characterize our graphene sample before doing doping. The near field image in Fig. 19 is an graphene on SiO2 without doping. In order to determine the wavelength of the plasmon localized on the boundary. We extract the profile of near field amplitude of the line draw perpendicular to the edge. The wavelength of the plasmon for this undoped sample is evidently about 240nm. It is consistent with theoretical value and also the value reported by other groups(see Fig. 8). Next, we begin expose the sample in UV in atmosphere to generate ozone on the surface of the sample for 5mins. The results are shown in 21 along with the data after annealing in air sequentially.

The effect of exposing graphene in UV ozone is evidently shown by [8]. In their raman study, they found that if graphene expose in ozone for time longer than 8-10mins, stronger bonding between carbon and oxygen starts to form
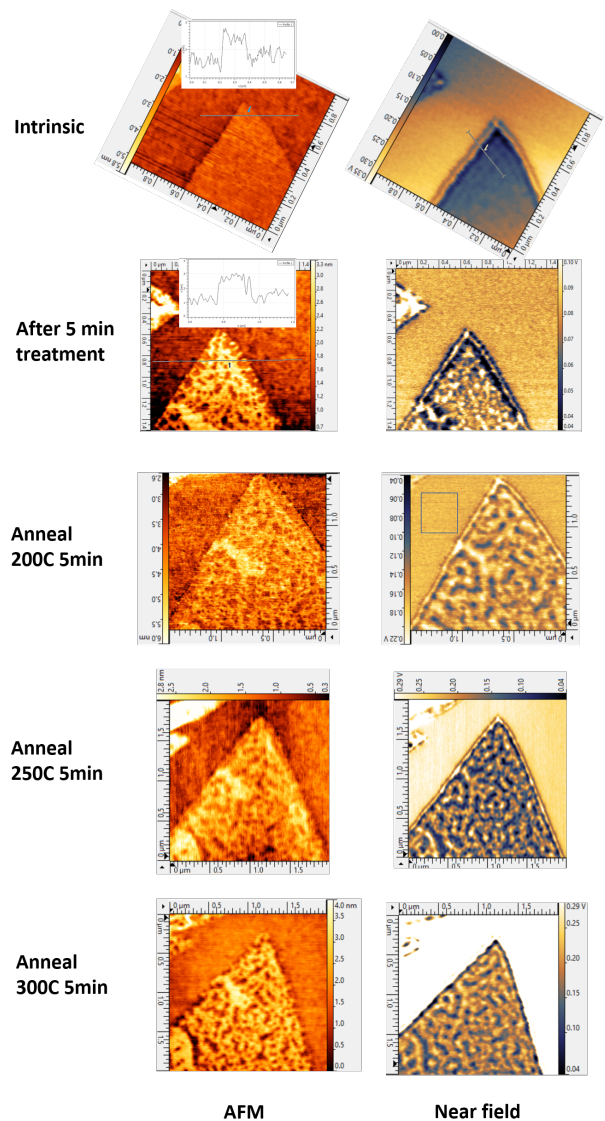
Figure 19: AFM (left) and near field (right) of graphene in sequence of 5 min UV ozone, annealing for 5 min with 200C, 250C and 300C. The intrinsic graphene shows very uniform near field signal in the interior. The AFM image shows sample height of around 1nm (bilayer graphene) and with roughness of order of 0.4nm. After UV ozone for 5min, the sample roughness increased to ∼0.8 and in some location height is increased. The near field after UV ozone shows robust plasmon fringes interference in the interior, and very strong fringe on the edge. All the near field image are normalized in same scale for comparison. Then the sample is annealed in air for 200C, 250C and 300C. As annealing temperature increases, the visibility of plasmon fringes in the interior decreases and but the width of the fringes seems to increase indicating an improvement of sample quality. There also small changes to the AFM images, the changes might because of the evaporation of some O3 ion.
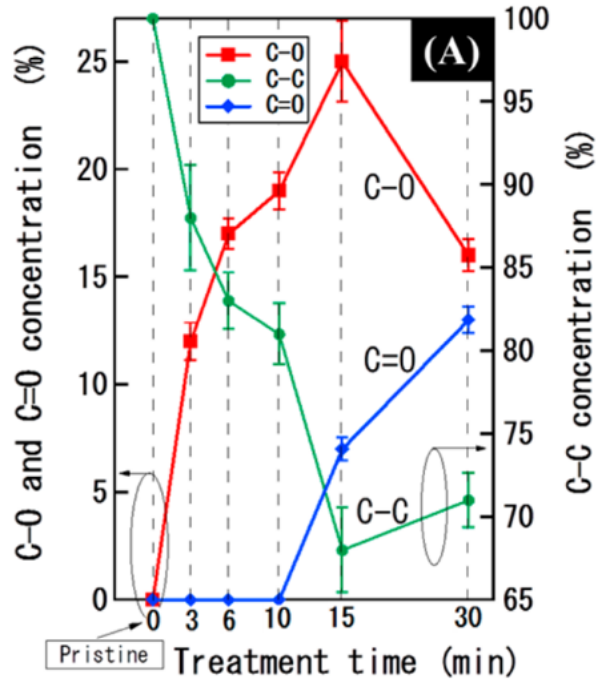
Figure 20: UV ozone treatment time and C-O C-C and C=O concentration as a function of treatment time. As shown in the graph, C=O bond does not form until 10-15mins. C-0 bond forms relatively easy and at 3 min treatment the concentration of C-O is about 12% and the slope is relatively linear until 8-10min implying doping rate of 4%/min (This image is obtained from Y. Mulyana 2014) [8]

(double bonds) and the bonding energy is 0.25ev which corresponding 3000 kelvin thus, cannot be removed by annealing. however, alternatively, they had shown that it can be reduced by shining UV light on it. This study suggest, in our sample, the effect of plasmon fringes we saw was coming from C-O bonds and one can have fine control over the doping level. and the reduction process with UV light should in theory can reduce small percentage of doping level to,very close to, pristine states.

However, our AFM image and near field study of 5 min ozone suggest that annealing in high temperature is not sufficient to break C-O bond and the surface of the sample seems to be damaged and cannot reverse back to
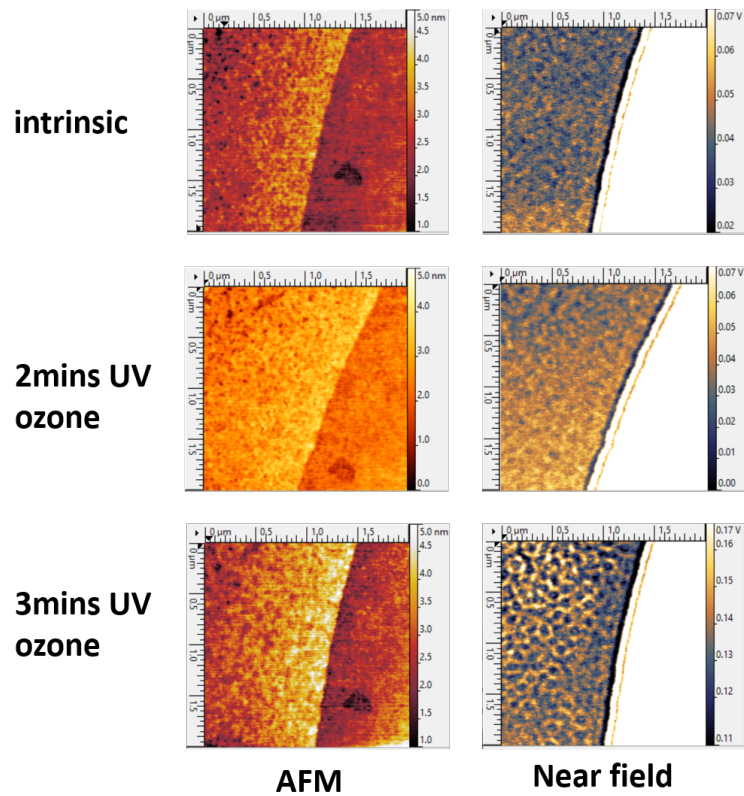
Figure 21: AFM and near field image of series of treatment for graphene on SiO$_2$. Intrinsic graphene is treated with UV ozone in sequent of 2 mins and 3 mins. There is a slight change in the interior of the graphene for 2 min treatment and obvious change after 3 min of treatment. There is no sign of change in topography from AFM image which shows very promising way of generating plasmon on in the interior without damaging the graphene. Further optimization of the system to obtain better control and lesser effect on topography can be achieved.

pristine condition. It is natural to try again in another direction, that is, to dope the sample with increase of time interval to search the condition at which the sample has no physical damage while doping level is still significant to generate plasmon puddles. The following experiment is done and the result is shown in 22. Another clean flake of graphene (bilayers) is prepared and characterized before doping and is then UV ozone sequentially for increasing amount of time interval. 2mins of irradiation time has no obvious change in near field or topography, however, a large change when irradiate again for 3mins. An important thing to note here is that the total irradiation time is 5mins, however, is not linear in this small time interval regime. It seems like there is no doping effect for time less than 1-2mins (this is similar principle as to microwave food the molecules will need some time to reach the most energized, resonant, condition). We had constructed another testing to verify this hypothesis. A sample is exposed for 1mins and for 3 times with UV ozone and compare to another sample UV ozone for 3mins directly. The result is, there is a different in them, the sample exposed 3 times looks like intrinsic states while the sample expose for 3min continuously will shows plasmon puddles similar to 22.Indeed, there exist a minimum amount of time to be able to dope the sample and is where we can potentially use this to create a very fine/ doped graphene and with minimum amount of damage on it.

In our previous annealing study of 5min exposure time in UV ozone. The sample is annealed again at a rather high temperature, 500C, for 6mins. After annealing, unexpected and interesting feature appeared. See 23). Plasmon rings around a bright center appear which appear usually in defects and a small grain size. Normally, the grain and defect will have less conductance than the graphene sheet and thus, acting like a physical boundary for electron density wave and creates interference pattern around the defect.Also, if the defect/gain is much smaller than the plasmon wavelength, the reflectance of plasmons will small and resulting no detection of plasmon.This, on the other hand has plasmon rings and also a plasmon mode at the center of the rings which suggest it might not be a defect on the lattice side but rather, seems like there is resonant on the center. One of the key observation here is that there are many robust fringes one can see, much more visible than even a physical boundary of a triangle shape in the same sample. This suggest it might be some resonant there otherwise it will at most create the reflection pattern (as from physical boundary of a circle) and with visible fringes or 2 and with center as dark spot. There are few possibility that can create a resonant as mentioned in reference [7], one can place two graphene
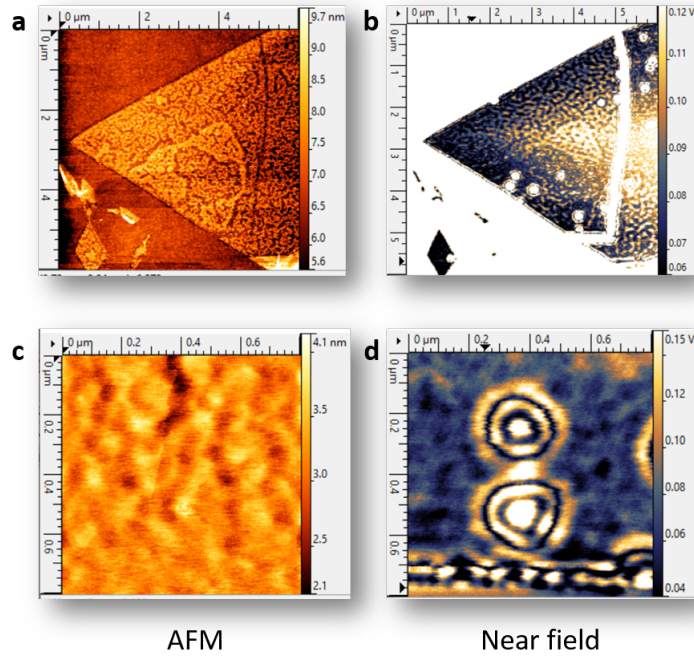
AFM   Near field

Figure 22: AFM and near field image of graphene annealed again for 6min in 500C. It is the same sample as 21 unexpected plasmon rings around a bright center appeared suddenly (see d). a. topography doesnt have dramatic change compare with before annealing. b. robust plasmon puddles are still there in the interior of the graphene and the size of the plasmon puddles seems increased. c and d. small area scane of a plasmon rings around a defect/dopant. There is no topography correspondent at the center of the plasmon rings and the center is bright. suggests the size of the defect might be small and the defect is more conducting locally rather than insulating/poor conductance. the latter is because for an poorly conducting/insulating defect/grains, the center of the spot will be dark this will become more obvious as we see more evident later

42

sheet very close together and the SPPs from both sheet reaches out and resonate for specific parameters. Another possibility is that as mentioned in the theoretical paper of p-n junction [5], For a potential well of width 2d, plasmon can travel into the potential well and form modes inside the with 2d if the plasmon wavelength is much larger than 2d. Although there is no evident, so far, what it might be, this is exotic and finding out the mechanism might be fundamentally important to other study and plasmonic applications. Even though the possibility of the defect being a resonator is favored, for it being a defect with higher or lower conductivity in the center of the plasmon rings is possible with non negligible probability. The number of visible plasmon rings is not high enought to tell the different from being just a physical boundary. A resonator might produce much more fringes than one can expect from a physical boundary. There is a theoretical study of graphene plasmon propagate across a defect that suggest the wavelength of plasmon will be depend on the size of the defect. [9]. In their calculation, they considered different kind of defect. For example, a poorly conducting one,a highly conducting one and a insulating one. As in the insulating case, his calculation shows if the size of the defect is larger than 0.1λ, then the plasmon wave will be reflected completely. See Figure 24. The size of a is larger than the value indicated and the plasmon fringes reflected from the defect completely. It matches the theoretical prediction and the dark spot appear after further annealing with 600C and for 6mins. Another point the calculation shows, for a poorly conducting defect, they found plasmon wavelength scale with defect size such that $\lambda_p/a \approx 2\pi/\sqrt{2} \approx 4.44$, This also agree quite well with our results. See 25. the ratio for two different plasmon ring is about 2 and 4.8. it is important to note that in the theoretical calculation, they had assumed a few setting that are different from our case and are crucial that will change the result. One thing is that they had consider a infinite strip and we have, likely, a circle. and they didn't account for radial component of plasmon because they have perfectly flat sheet and we have roughness on surface which might not be negligible, even though, in general it's a small contribution and our roughness is of the order of 1nm.

In conclude of defect study, accounting all the evident. It seems like annealing graphene in air for 500C will create poorly conductive defects (might not be physical holes because otherwise will show up in AFM, unless it's too small but for small holes the plasmon reflection is small and should not give rise to such robust plasmon ring) and as anneal further, the defect grows larger and forming completely insulating grain and reflect all the plasmon
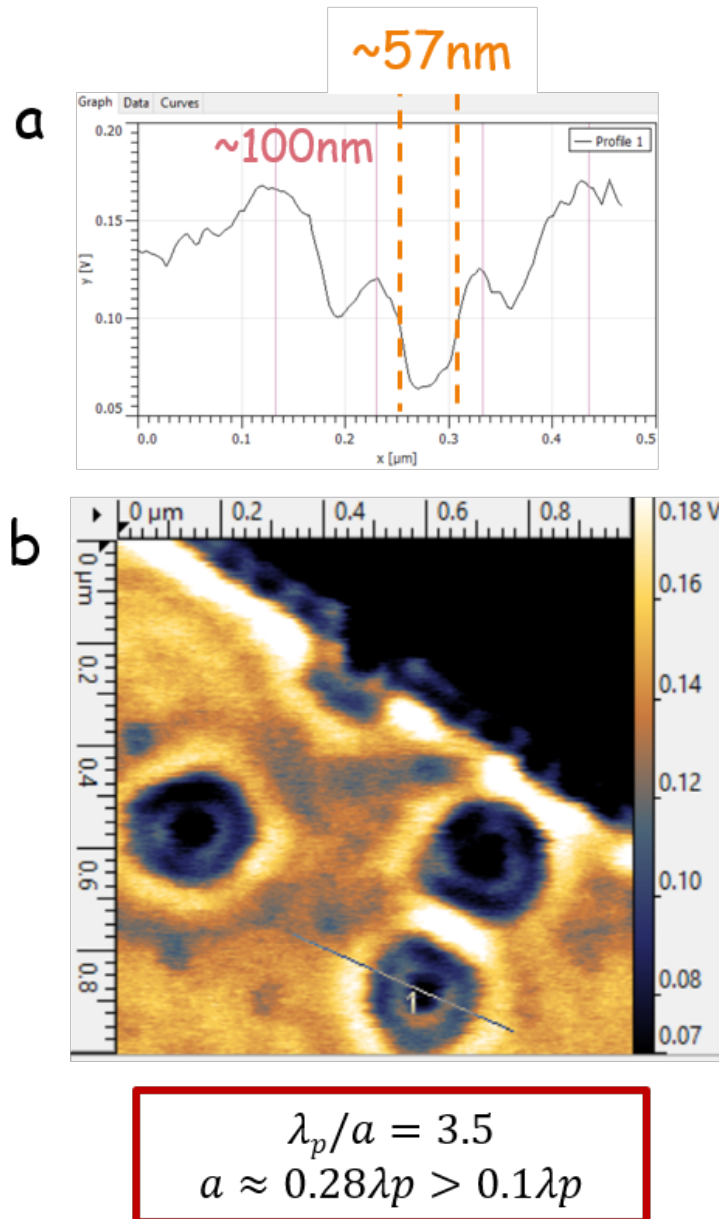
Figure 23: Near field image of a dark defect b. (annealed again with 550C for 6mins) and a. the profile extracted on the line across a dark defect. The plasmon wavelength is about 200nm and the size of the defect is about 57nm the ratio. $a \approx 0.28\lambda_p > 0.1\lambda_p$
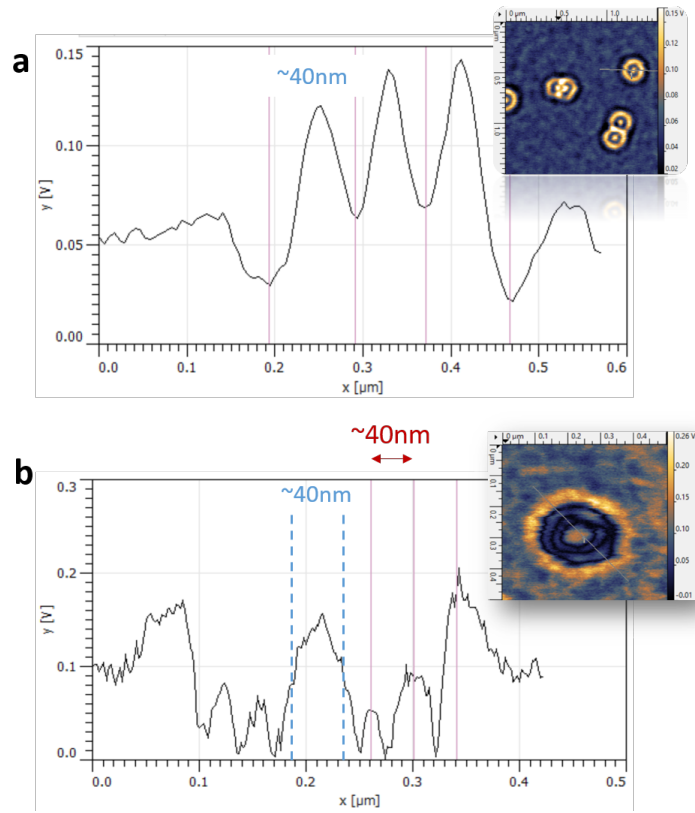
Figure 24: two more defect image with bright center. a. profile of line across the plasmon ring shown as insert. profile of the line across another plasmon ring circle shown as insert. the wavelength of figure a and b are approximately the same (40nm) but the FWHM of the center is different giving rise of a. and b. $\lambda_p/a \approx 4.8$

wave forming plasmon fringes.The actual mechanism and formation of such defect need to be studied further in order to understand it. annealing in nitrogen/argon gas instead of air will certainly can identify if the graphene is oxidized, and/or UV ozone for just enough time to build C=O double bone to see how it would be differ from C-O bond in graphene plasmon.

Chapter 6   Conclusion and Outlook

In short conclusion, infrared plasmon in graphene has many unexplored corner waiting to be illuminated. There are many possibility and potentials one can achieve by exploring in both experimental and theoretical direction. Graphene plasmon guide with p-n junction is a simple idea and is achievable with enough efforts. The theoretical calculation has shown promising results [5] - electron density wave can be controlled by potential wall created with p-n junction but different scenario comes into account and fine turning of the width of the junction is important. One should first understand and design a reasonable junction width to achieve the desired boundary condition for plason fringes. Possible reason of no plasmon fringes observed at the physical boundary of sandwiched graphene should be addressed and solve. The bubble issue can be further improve by the details of each small steps. Having least amount of residue on substrate and not to strain the hBN or other flakes while stacking. Choices of crystal flakes also evidently plays an important role of amount of bubbles. Thicker crystal tend to be have less bubble and wrinkle since they are firmer. Also bubbles can be introduced as each stack process and thus, designing an hetero-structure that requires least amount of steps will greatly improve the quality. Lastly, the environment during stacking can be improve by controlling the humidify and dust concentration on air, vacuum space environment is ideal. oxygen doping of graphene has shown great potential in creating plasmon in the interior of the graphene and one can dope with different amount to fine tune the carrier concentration or defect size to change the wavelength of the plasmon. Together with masking, one can show a generation of plasmon circuit with various masking size and the plasmon might form different modes with respect to the size of the propagation circuit. Uniformness will play a crucial role in such plasmon circuit and the ideal case is to pattern periodic strips with various sizes and irradiate with ozone might resulting coupled plasmon modes and propagate in unlimited distant. Thus, breaking the need of physical boundary condition to generate such plasmon circuit. This can be ground breaking to plasmonic applications if one can easily achieve making such plasmon circuit by just masking and irradiate with UV ozone. Another possibility is to generate a pseudo magnetic field in graphene via strain by UV ozone with some small particle density on the graphene and then place another layer of graphene on top. This will be bilyer or trilayer graphene that can still generate plasmon and resonant might happen between the graphene sheets because the top

47

and bottom graphene has same electornic property and the physical dopant of oxygen are between the layer. This will require the sandwiched oxygen to form same interaction between top and bottom graphene which might be achieve by annealing because as we had seen, for short exposure time of ozone, the graphene can be reduce back to intrinsic condition which means the energy of provided from annealing is enought to break the interaction of oxygen and graphene. Thus, the oxygen between the sheets can decouple from bottom graphene and form a more stable interaction between the two atomic sheet. by controlling the amount of oxygen doped, one can introduce stain on top graphene and thus introduce a high pseudo tesla magnetic field and quantize the electronic states on the oxygen strain and might show up in the near field imaging. [10]. As we mentioned before that the oxygen bond can be reduce by shining UV light on it, thus can also be used to move the oxygen between the sheet to a lower energy configuration for plasmon resonant study. This has advantage over annealing because of it does not damage the graphene at all. Annealing in high temperature evidently does change the graphene property which might introduce new effects. Shining UV light on graphene protected oxygen layer might generate a layer of 2D oxygen plasma between the sheet and might have interesting application or effects. beginfigure

One can also capsulize oxygen with graphene-hBN stack. Evidently, the uv plasmon does attach to the surface of hBN quit well and eventually forming a layer of oxygen. 26, the hBN is treated with UV ozone for 6min is then emerged in accetone for 15min and heated up to 200C for 6min. Before the treatment the surface of the hBN is flat (data not shown) and after the treatment the residue like spot show up. It is more likely that the residue is oxygen attachment because the same chemical treatment of hBN but without UV ozone was done and no residue on hBN was observed. I believe, initially, the UV ozone attach uniformly on the surface of hBN as UV irradiate for some longer time stronger bond starts to form and annealing reduce most oxygen but cannot remove strongly bonded oxygen. similarly to graphene UV ozone process. This should be verified and my believe was based on the observation of, uniform surface of hBN after short amount of UV time (1.5min) and residue like spot appeared after the treatment mentioned above. unfortunately, the data after UV 1.5min (and without annealing) treatment was buried in a huge pile of data. Thus, one can utilize this to form a uniform oxygen layer between hBn and graphene and then irradiate with UV again without expose in oxygen to form a layer of oxygen plasmon between and
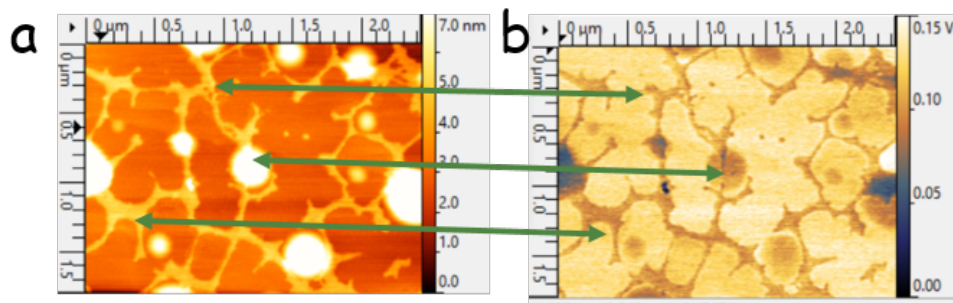
Figure 25: AFM and near field image on the surface of hBN. The bright spot on the AFM image are imaged as dark spot on the near field as indicated with correcsponding green arrows. The signal of valleys are due to topography effect of the height spot on the hBN. This is after treatment of UV ozone and dipped under accetone for 15min and is then heated up for 200C for 5 min. and evidently, UV ozone attach on the surface of hBN and forming residue like on the surface of hBN

forming a more stable doping effect. I would expect the oxygen form bonding on hBN rather than on carbon but still can introduce localized doping on the graphene sheet. to see the effect, one might need to do treat in UV ozone of hBn of longer time to increase the strength of the oxygen hBN bonding and rhus when uv again, the strongly bonded oxygen will not be activated until a longer time while the weaker bonded oxygen will interact with graphene creating uniformed interaction on the graphene sheet, resulting contrast and, hopefully, potential boundary to observe plasmon puddles.

Lastly, one can also utilize the supreme electronic property of suspended graphene and create circle like defect from systematic annealing process and might see robust fringes develop around defects to extract more information about the mechanism of the system.

References

[1] Andreev, G. Beating the Diffraction limit by 1000X. Bruker Present. (2013).

[2] Liu, W. J. et al. Characteristics of a Single-Layer Graphene Field Effect Transistor with UV/Ozone Treatment. ECS Solid State Lett. 2, M1M4 (2012).

[3] Leconte, N., Ordejo, P., Tao, H. and Bachtold, A. Damaging Graphene with Ozone Treatment- A Chemically Tunable MetalInsulator Transition.pdf. 4, 40334038 (2010).

[4] Fei, Z. et al. Gate-tuning of graphene plasmons revealed by infrared nano-imaging. Nature 487, 8285 (2012).

[5] Mishchenko, E. G., Shytov, A. V. and Silvestrov, P. G. Guided plasmons in graphene p-n junctions. Phys. Rev. Lett. 104, 15 (2010).

[6] Chen, J. et al. Optical nano-imaging of gate-tunable graphene plasmons. Nature 15 (2012). doi:10.1038/nature11254

[7] Jablan, M., Soljacic, M. and Buljan, H. Plasmons in Graphene: Fundamental Properties and Potential Applications. Proc. IEEE 101, 16891704 (2013).

[8] Mulyana, Y., Uenuma, M., Ishikawa, Y. and Uraoka, Y. Reversible oxidation of graphene through ultraviolet/ozone treatment and its non-thermal reduction through ultraviolet irradiation. J. Phys. Chem. C 118, 2737227381 (2014).

[9] Garcia-Pomar, J. L., Nikitin, A. Y. and Martin-Moreno, L. Scattering of graphene plasmons by defects in the graphene sheet. ACS Nano 7, 49884994 (2013).

[10] Levy, N. et al. Strain-induced pseudo-magnetic fields greater than 300 tesla in graphene nanobubbles. Science 329, 544547 (2010).

[11] Barnes, W. L., Dereux, A. and Ebbesen, T. W. Surface plasmon subwavelength optics. Nature 424, 82430 (2003).

[12] Barnes, W. L. Surface plasmonpolariton length scales: a route to sub-wavelength optics. J. Opt. A Pure Appl. Opt. 8, S87S93 (2006).

[13] V. Jean-Yves Y. Flix, B. Ivn, Atomic-scale control of graphene magnetism by using hydrogen atoms (E. 845, (2014).